

Mechanism of dynamic nuclear polarization in high magnetic fields

C. T. Farrar, D. A. Hall,^{a)} G. J. Gerfen,^{b)} S. J. Inati,^{c)} and R. G. Griffin

Francis Bitter Magnet Laboratory and Department of Chemistry, Massachusetts Institute of Technology, Cambridge, Massachusetts 02139

(Received 29 March 2000; accepted 14 December 2000)

Solid-state NMR signal enhancements of about two orders of magnitude (100–400) have been observed in dynamic nuclear polarization (DNP) experiments performed at high magnetic field (5 T) and low temperature (10 K) using the nitroxide radical 4-amino TEMPO as the source of electron polarization. Since the breadth of the 4-amino TEMPO EPR spectrum is large compared to the nuclear Larmor frequency, it has been assumed that thermal mixing (TM) is the dominant mechanism by which polarization is transferred from electron to nuclear spins. However, theoretical explanations of TM generally assume a homogeneously broadened EPR line and, since the 4-amino TEMPO line at 5 T is *inhomogeneously* broadened, they do not explain the observed DNP enhancements. Accordingly, we have developed a treatment of DNP that explicitly uses electron–electron cross-relaxation to mediate electron–nuclear polarization transfer. The process proceeds via spin flip–flops between pairs of electronic spin packets whose Zeeman temperatures differ from one another. To confirm the essential features of the model we have studied the field dependence of electron–electron double resonance (ELDOR) data and DNP enhancement data. Both are well simulated using a simple model of electron cross-relaxation in the inhomogeneously broadened 4-amino TEMPO EPR line. © 2001 American Institute of Physics.

[DOI: 10.1063/1.1346640]

I. INTRODUCTION

During the last decade, the repertoire of methods to perform structural studies with solid state NMR (SSNMR) has expanded considerably. There are now multiple methods to measure distances,¹ torsion angles,² and otherwise constrain molecular structure. Furthermore, many promising applications of these methods have appeared. Nevertheless, when compared to solution NMR, the sensitivity of SSNMR experiments is lower by two to three orders of magnitude per unit time. The reason for this decreased sensitivity is that SSNMR experiments generally involve the direct detection of low gyromagnetic ratio (γ) nuclei, ¹³C, ¹⁵N, ³¹P, etc., rather than indirect detection via the more sensitive ¹H spin as in solution NMR. To address this problem we are exploring the possibility of performing dynamic nuclear polarization (DNP) experiments^{3,4} to improve the sensitivity of SSNMR. For example, we have recently obtained DNP SSNMR signal enhancements of up to 400 at high magnetic field (5 T).^{5–7} These signal enhancements could have dramatic consequences, particularly for the study of biological systems where sample quantities and signal to noise are often severely limited.

DNP involves irradiating the EPR spectrum of either endogenous or exogenous electron spins at or near their Larmor frequency, and thereby transferring the large electron spin

polarization to nuclear spins. In principle, signal enhancements on the order of γ_e/γ_n , corresponding to a factor of ~ 660 for ¹H nuclei and ~ 2600 for ¹³C nuclei, are obtainable. However, two factors have impeded the application of DNP to high field, high resolution SSNMR—the absence of high frequency, high power microwave sources to drive the polarization transfer and a dearth of understanding of the mechanism of DNP at high fields. We have addressed the first problem with the development of high power (1–25 W) gyrotron microwave sources operating at 140 GHz (5 T) (Refs. 5, 8) and 250 GHz (9 T).⁹ In this paper, we address the second problem with a detailed investigation of the mechanism of electron-to-proton polarization transfer in the 4-amino-TEMPO/water/glycerol system.

The DNP mechanism usually operative when a nitroxide radical is the polarizing agent is thermal mixing (TM),^{10–13} which can be understood using a formalism in which the electron–nuclear spin system is described as a set of three interacting baths. In particular, the three baths are the electron Zeeman system (EZeS), the electron dipolar system (EDS), and the nuclear Zeeman system (NZS), each of which is described by a spin temperature (Fig. 1).^{11,14} TM proceeds through a two-step process driven by off-resonance irradiation of the allowed EPR transition that produces a large, nonequilibrium polarization gradient across the EPR line. Production of this gradient is equivalent to cooling the EDS (Fig. 2). Second, a thermal contact between the EDS and NZS cools the nuclear system via energy conserving three-spin, electron–electron–nuclear exchange process (Fig. 3).^{15,16} This three-spin process requires that the homogeneous width of the EPR line (δ) be greater than the nuclear Larmor frequency (ω_n).

^{a)}Present address: Dean and Company, 8065 Leesburg Pike, Vienna, Virginia 22182.

^{b)}Present address: Department of Physiology and Biophysics, Albert Einstein College of Medicine, Bronx, New York 10461.

^{c)}Present address: Center for Cognitive Neuroscience, Dartmouth College, Hanover, New Hampshire 03755.

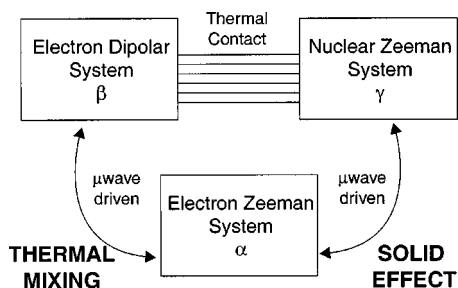


FIG. 1. Thermodynamic model used to describe DNP in a system exhibiting a single homogeneous EPR line at a low magnetic field strength. The solid effect is driven by direct irradiation of electron–nuclear transitions, while thermal mixing is mediated by the electron dipolar system (EDS). The parameters α , β , and γ are the inverse spin temperatures which describe the populations of their respective thermodynamic baths.

While the theory of TM is well understood at low fields, little is known about the details of the mechanism in the regime encountered at high fields where additional factors become significant. First, the high field EPR spectrum rarely consists of a homogeneously broadened line whose shape is governed by electron–electron dipolar couplings. Instead, the spectral line shapes are dominated by the g -anisotropy that is primarily inhomogeneous in nature. Under these conditions, the hypotheses of a single electron Zeeman spin temperature is not valid, and microwave irradiation results in hole-burning rather than uniform excitation of the spectrum. A second consequence of the dominance of the g -anisotropy

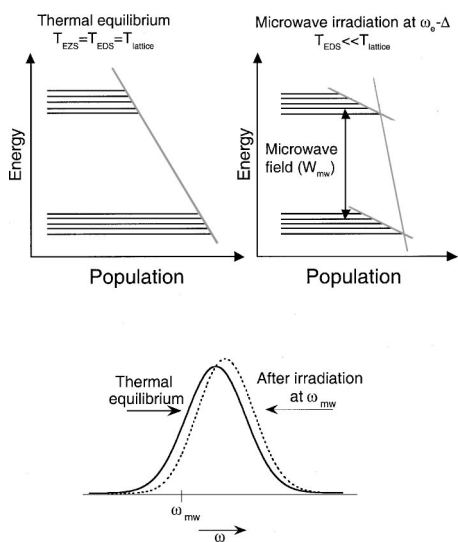


FIG. 2. (Top) Population diagram of a homogeneously broadened spin-1/2 EPR line. The two bands in each diagram correspond to the populations of the upper- and lower-EPR manifolds. The broadening of each level is assumed to derive from electron–electron dipolar interactions. The left diagram illustrates the thermal equilibrium condition, in which the EDS and EZS are at the same temperature as the lattice. The right diagram shows the effect of microwave irradiation downfield of the center of the EPR line. The mismatch ($\Delta = \omega_e - \omega_{mw}$) between the Larmor frequency of the electron and the microwave frequency results in a dynamic cooling of the EDS, and hence a large polarization gradient within each manifold, while the Zeeman spin temperature remains at approximately its thermal equilibrium value. (Bottom) The EPR absorption spectrum which would be observed before (solid trace) and after (dashed trace) microwave irradiation corresponding to the two energy diagrams above.

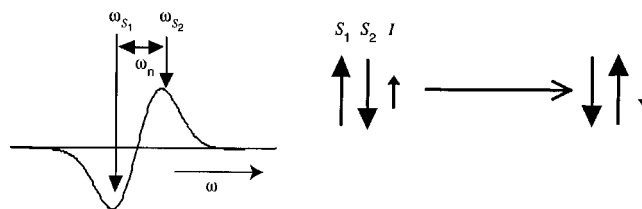


FIG. 3. Diagram illustrating the process by which thermal mixing proceeds. (Left) A large polarization gradient across the EPR line is established by off-center microwave irradiation, representing the difference between the thermal equilibrium lineshape and the microwave irradiated line shape (see Fig. 2, bottom). (Right) Energy-conserving (S_j) three-spin flip–flop processes involving two electronic spins (S_1 and S_2) and one nuclear spin (I) then drive the high polarization of the electron dipolar bath to the nuclear manifold.

is that the assumption that the nuclear Larmor frequency (ω_n) is less than the homogeneous EPR linewidth (δ) is often invalid, suggesting that the thermal contact between the electrons and the nuclei does not necessarily proceed via the dipolar system of the electrons. As an illustration of this point, we note that at 5 T fields we observe no significant polarization enhancement attributable to thermal mixing for samples of the free radical α - γ -bis(diphenylene)- β -phenylallyl (BDPA) doped into polystyrene at room and low temperature.^{5,8} The BDPA EPR line (which is effectively homogeneous when the radical concentration is reasonably high) is much narrower ($\omega/2\pi \sim 20$ MHz) than the ^1H Larmor frequency ($\omega_{\text{H}}/2\pi = 211$ MHz). As a result, the probability of a three spin electron–electron–nuclear flip is negligibly small, resulting in an extremely weak thermal contact between the ^1H spins and the electron spins. In comparison, at lower magnetic fields (≤ 1.4 T), the BDPA linewidth is on the order of the nuclear Larmor frequency and a sizable thermal mixing enhancement is observed.^{12,13}

Nevertheless, TM is not necessarily precluded for an inhomogeneously broadened EPR line. As first suggested by Bloembergen *et al.*,¹⁷ electron–electron cross relaxation across an inhomogeneously broadened EPR line can render the line effectively homogeneous over sufficiently long time scales. In the case of rapid cross-relaxation, the entire broadening, both inhomogeneous and homogeneous, of the EPR line can be considered to form a bath characterized by a single spin temperature (Fig. 4) and the EPR line will behave as if it were effectively homogeneous.^{18–21} If ω_n is less than the EPR broadening, this so-called electron broadening system (EBS) would sustain a coupling to the nuclear spins and the DNP dynamics would closely mirror the homogeneous line case.³ However, since our DNP experiments are performed at both a high magnetic field strength (resulting in increased inhomogeneous contributions) and at moderate temperatures (leading to faster electron spin-lattice relaxation), the assumption of fast cross-relaxation across the 4-amino-TEMPO EPR line does not necessarily hold. In this case the simple three-bath model no longer adequately describes the polarization transfer dynamics. Instead, the coupling between the electronic and nuclear spins proceeds via pairs of electronic spin packets, spaced ω_n apart and whose

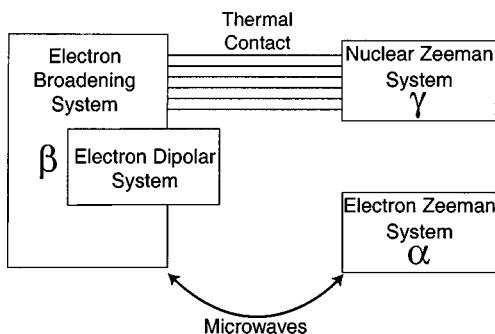


FIG. 4. Thermodynamic model used to describe thermal mixing in an inhomogeneously broadened EPR line with fast cross-relaxation. The model is similar to that for a homogeneously broadened line, except the non-Zeeman electronic reservoir is comprised of interactions characterizing the homogeneous and inhomogeneous EPR broadening. The state of the entire broadening system is described by a single parameter $\beta = 1/kT_{\text{EBS}}$. In this model, if the EPR linewidth is at least on the order of the nuclear Larmor frequency, then an electron–nuclear thermal contact can exist, coupling the electron broadening system (EBS) to the nuclear Zeeman system (NZS).

Zeeman temperatures can differ from one another.

In this paper we describe the results of a number of DNP, electron–electron double resonance (ELDOR), and electron saturation–recovery experiments which illustrate the effect of electron–electron cross-relaxation on the spin dynamics of the 4-amino-TEMPO system during low-power microwave irradiation at 5 T. These experiments indicate that cross-relaxation plays a significant role in facilitating DNP, but that the assumption of a pseudo-homogeneous EPR line fails under typical experimental conditions. We therefore explicitly include the cross-relaxation process in a spin-temperature model of the hole-burning and polarization transfer dynamics, and use this model to simulate the salient features of ELDOR and DNP in the 4-amino-TEMPO system.

II. EXPERIMENT

A. Sample preparation

Samples consisted of various concentrations of the nitroxide free radical 4-amino TEMPO (4-amino-2,2,6,6-tetramethyl-piperidine-1-oxyl) dissolved in a 60:40 glycerol/water solution. For DNP/NMR experiments, $\sim 120 \mu\text{l}$ of solution was placed in a $\sim 4 \text{ mm}$ o.d. quartz tube. The samples underwent several freeze–pump–thaw cycles to remove dissolved O_2 , which can increase the rate of electronic and nuclear spin-lattice relaxation, and were then sealed. The EPR samples were loaded into quartz capillary tubes with o.d.’s ranging from 0.55 mm for low concentration ($< 10 \text{ mM}$) samples to 0.16 mm for concentrated samples. The smaller diameter tubes are required for highly concentrated samples to minimize sample susceptibility effects. The EPR samples were degassed and sealed as described above for the NMR samples.

B. Microwave sources

High-power DNP and ELDOR experiments utilized a 139.64 GHz gyrotron source, described previously by Becerra *et al.*,⁵ which has been optimized for DNP applica-

tions. DNP experiments based on the solid effect and thermal mixing generally require pulses on the order of the nuclear T_1 (\sim seconds). This gyrotron is capable of $\sim 100 \text{ W}$ output power under quasi-CW conditions (60% duty cycle) and $\sim 10 \text{ W}$ under CW operation, with a frequency stability of $\sim 2 \text{ ppm}$. Low power DNP was performed with the 139.5 GHz Gunn diode of the EPR spectrometer (output power 10 mW). The Gunn diode source is injection locked by a 15.5 GHz DRO that is in turn locked to a 50 MHz crystal oscillator (-150 dBc/Hz at 1 kHz offset).

C. Dynamic nuclear polarization NMR

DNP/NMR experiments were performed on a custom designed 211 MHz spectrometer⁵ employing a heterodyne mixing scheme with an intermediate frequency (IF) of 120 MHz. All DNP data were acquired with a two-channel transmission-line probe capable of operation at temperatures from 10 to 300 K. DNP is performed using either a 139.50 GHz Gunn diode (10 mW) or a 139.64 GHz gyrotron ($\sim 10 \text{ W}$) to drive the polarization transfer. A WR-42 waveguide delivers microwaves through the length of the probe. Near the sample, the waveguide tapers to WR-8, and the microwaves are launched between turns of the NMR coil. Transmission to the sample leads to approximately 10 dB of attenuation, resulting in incident powers at the sample of 1 mW for the Gunn Diode source and 1 W for the gyrotron. The microwave Q of the static DNP probe is low ($Q \sim 1$), which limits the amplitude of the microwave B_1 field. However, the advantage of this design is that the optimal Q and filling factor of the NMR system is retained since the rf circuitry is unperturbed by the microwave components.

^1H DNP enhancements were measured via saturation recovery experiments. After a long ($\sim 5 \text{ ms}$) RF saturation pulse and a delay T , the nuclear polarization is measured via a solid echo pulse sequence ($90_x - \tau - 90_y - \tau$). The DNP enhancement ϵ is defined as $\epsilon = (I_{\text{mw}}/I_0) - 1$, where I_{mw} and I_0 are the signal intensities with and without CW microwave irradiation. Signal intensities were also measured with microwave irradiation completely off-resonance with the EPR line to control for heating effects.

D. Electron paramagnetic resonance

The CW and pulsed EPR measurements were performed on a custom designed 139.50 GHz EPR spectrometer, which has been described previously.⁵ The spectrometer utilizes quadrature detection and a large-bore magnet centered at a field value of 4.974 T with a $\pm 75 \text{ mT}$ superconducting sweep coil and field lock system.²² Microwave $\pi/2$ pulse lengths of $\sim 400 \text{ ns}$ are obtained with a 10 mW Gunn diode source (Millimeter-Wave Oscillator Co.), a high-speed microwave switch (Donetsk Physico-Technical Institute, 7 dB insertion loss), and a cylindrical resonant cavity operating in the TE_{011} mode with a loaded Q of 500–750. A pulse programmer with 4 ns time resolution (Interface Technology) controls the microwave switches. The software controlling the EPR spectrometer is written in the LabVIEW environment and data is collected with a boxcar averager. Electron spin-lattice recovery times are measured using a saturation-

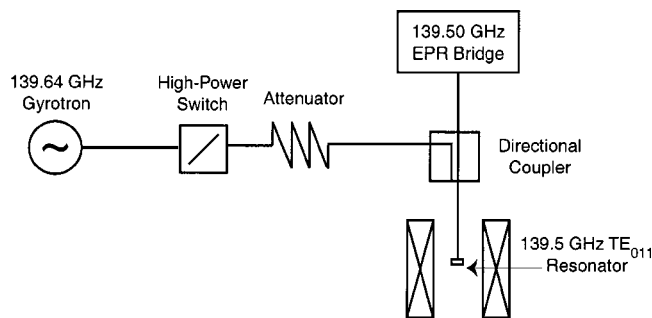


FIG. 5. Block diagram of the experimental set-up used for the high-frequency ELDOR measurement. Microwaves from the 139.64 GHz gyrotron source are switched and attenuated before entering the 139.50 GHz channel via the reflected power port on a 20 dB directional coupler. The 139.64 GHz channel does not affect the sensitivity 139.50 GHz EPR detection channel.

recovery pulse sequence. After a long saturation pulse (1–60 ms) and a variable delay T , a three-pulse stimulated-echo pulse sequence is used to monitor the recovery of the electron magnetization.

E. Electron–electron double resonance (ELDOR)

Our implementation of the ELDOR experiment (Fig. 5) utilizes two fixed-frequency microwave sources: the 139.64 GHz gyrotron for excitation and the 139.50 GHz EPR bridge for detection. The ELDOR pulse sequence is shown in Fig. 6. After 139.64 GHz microwave irradiation for a time T followed by a delay τ , a three-pulse stimulated echo pulse sequence samples the polarization at 139.50 GHz. The intensity of the stimulated echo is monitored with a boxcar averager.

A prototype high-power (<10 W) microwave switch (Capitol Technologies), which exhibits 30 dB isolation and <3 dB transmission loss at 139.5 GHz, controls the 139.64 GHz microwave irradiation from the gyrotron. The gyrotron source is operated CW during the entire acquisition in order to eliminate the frequency drift at the beginning of a pulse due to gyrotron cavity heating. The microwaves then pass through a variable attenuator, which is required to avert the possibility of damage to sensitive components of the microwave bridge due to high microwave power levels. The excitation channel couples into the detection channel via the input port on a 20 dB directional coupler just outside the EPR probe. This implementation does not perturb the 139.5 GHz channel; the observed EPR pulse widths and echo intensities are unaffected by the additional channel. Although the cylin-

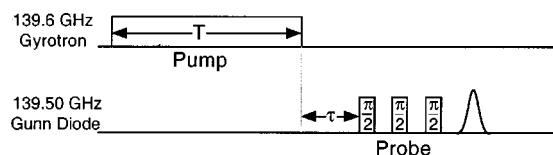


FIG. 6. Pulse sequence for the ELDOR experiment. The sample is irradiated with 139.64 GHz microwaves from a gyrotron source for a time T . After a delay τ , the stimulated-echo is measured with the 139.50 GHz EPR bridge. The 139.64 GHz channel is controlled by a high-power microwave switch and the gyrotron is run CW during the entire experiment to minimize frequency drift.

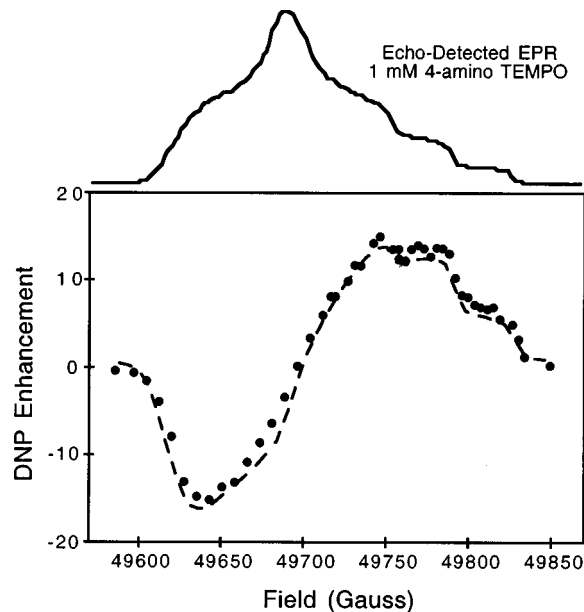


FIG. 7. Experimental data (circles) and simulation (solid trace) of the magnetic field dependence of the ^1H DNP enhancement for 40 mM 4-amino TEMPO in a 60:40 glycerol/water frozen solution under irradiation with the 139.50 GHz Gunn diode source at ~ 12 K. The echo-detected EPR spectrum of a 1 mM 4-amino TEMPO solution is shown above the graph. The parameters used in the simulations are $T_{1e} = 75$ ms, $T_{1D} = 25$ ms, $\omega_{10e}/2\pi = 20$ MHz, $W_{mw} = 0.0005$ MHz, and $W_{bb} = 25$ MHz.

drical resonator is tuned to 139.5 GHz in order to achieve maximal echo intensity, the coupling of the excitation channel is only ~ 3 dB less than the coupling of the detection channel, assuming that the resonator exhibits a Q of ~ 500 .

III. EXPERIMENTAL RESULTS

A. Field dependence of the DNP enhancement

Displayed in Fig. 7 is the dependence of the low power DNP enhancement on the external magnetic field strength along with the 1 mM 4-amino-TEMPO EPR spectrum. The 4-amino-TEMPO line shape is clearly inhomogeneously broadened—the principal electron g -values, corresponding to different molecular orientations of the nitroxide with respect to the magnetic field, are well resolved. A triplet structure, arising from ^{14}N hyperfine coupling, is observed on the high field edge of the EPR line. Despite the inhomogeneous nature of the EPR line, we observe maximal DNP enhancements of ~ 15 at 12 K with a low power (1 mW) Gunn diode microwave source. The triplet ^{14}N hyperfine structure evident in the high field edge of the EPR spectrum is also observed in the low power (1 mW) DNP field dependence. At higher microwave power (~ 1 W) this hyperfine structure is no longer observed in the DNP field dependence (data not shown).

B. Electron saturation recovery

Indirect evidence for electron–electron cross-relaxation in the 4-amino-TEMPO system is observed in electron saturation-recovery experiments. Figure 8 shows a saturation-recovery curve, acquired in the center of the EPR line (49 690 G) with saturating microwave pulse lengths of

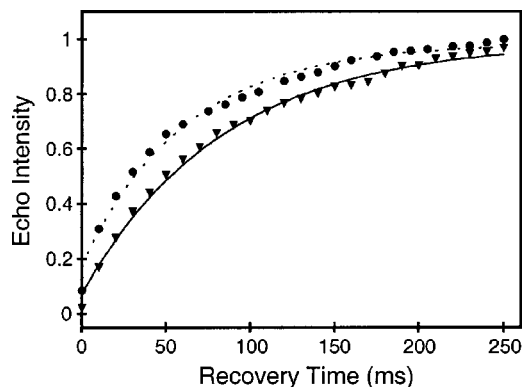


FIG. 8. Saturation-recovery EPR curves for 1 mM 4-amino TEMPO acquired at a magnetic field strength of 49 690 G, corresponding to the center of the EPR spectrum, and a temperature of 11 K. Saturating microwave pulses of 60 ms (triangles) and 10 ms (circles) were employed.

either 60 or 10 ms, for 1 mM 4-amino-TEMPO. Single exponential recovery curves are observed for both saturating pulse lengths with time constants approximately equal to the electron spin-lattice relaxation time ($T_{1e} \sim 75$ ms). The relaxation is slightly faster, however, with the 10 ms pulse than with the 60 ms pulse.

In contrast, saturation-recovery curves for 40 mM 4-amino-TEMPO, shown in Fig. 9, demonstrate a biexponential recovery that is sensitive to the saturating pulse length. For a short saturating pulse (1 ms), two relaxation components are observed; a fast component that can be attributed to cross-relaxation, and a slower component that can be attributed to pure T_{1e} relaxation. As the saturating pulse length increases (10 ms), the longer relaxation component begins to dominate, until, when the saturating pulse length is on the order of the spin-lattice relaxation time (60 ms), the recovery curves become single-exponential.

The saturation-recovery curve for 40 mM 4-amino-TEMPO is also sensitive to the magnetic field strength as demonstrated by a comparison of Figs. 9 and 10. In the former saturation-recovery is monitored at the low field edge of the EPR line (49 634 G), whereas in Fig. 10 the center of the EPR line (49 690 G) is monitored. The saturation-recovery curves for the low field edge of the EPR line vary substantially as a function of saturating pulse length until the

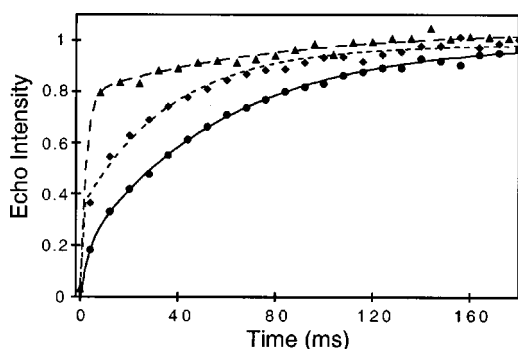


FIG. 9. Saturation-recovery EPR curves for 40 mM 4-amino TEMPO at 11 K and a magnetic field strength of 49 634 G, corresponding to the low field edge of the EPR spectrum. Saturating pulse lengths of 1 ms (triangle), 10 ms (diamond), and 60 ms (circle) were used.

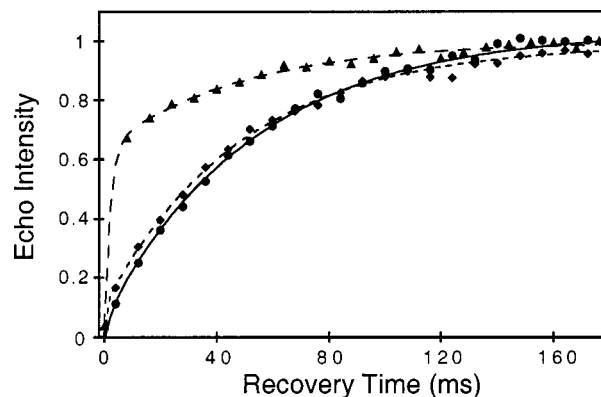


FIG. 10. Saturation-recovery EPR curves for 40 mM 4-amino TEMPO at 11 K and a magnetic field strength of 49 690 G, corresponding to the center of the EPR spectrum. Saturating pulse lengths of 1 ms (triangle), 10 ms (diamond), and 60 ms (circle) were used.

pulse is on the order of the spin-lattice relaxation time. However, when the center of the EPR line is irradiated, the recovery curves are invariant for much shorter saturating pulse lengths (≥ 10 ms). This suggests that, in the center of the line, the cross-relaxation time to most of the spin packets in the line is below 10 ms, while at the low-field edge, there is a dispersion of cross-relaxation times, up to the spin-lattice relaxation time. This effect is even more pronounced on the high field edge of the EPR spectrum (data not shown).

C. Electron–electron double resonance (ELDOR)

Perhaps the most direct observation of electron–electron cross-relaxation can be made using ELDOR experiments, the results being shown in Fig. 11. The ELDOR curve measures the attenuation of the electron spin echo at the 139.5 GHz probe frequency resulting from a 139.64 GHz pump pulse. The echo attenuation was measured as a function of the external magnetic field for two 4-amino-TEMPO solutions: the 40 mM solution, which yields substantial DNP enhancements, and a 1 mM solution where no DNP enhancement is observed and cross-relaxation is expected to be weak. For the 40 mM solution we observe significant attenuation of the electron spin-echo following the gyrotron pump pulse indicating that there is substantial cross-relaxation across the EPR line for this concentration of 4-amino TEMPO. In contrast, for the 1 mM solution we observe no significant attenuation at any field position, demonstrating that the effects observed in the 40 mM solution are unrelated to sample heating or other experimental artifacts. The large anisotropy in the attenuation of the electron spin-echo across the EPR line for the 40 mM 4-amino-TEMPO is consistent with the cross-relaxation rate being maximal in the center of the line, where the greatest density of spin packets resides.

IV. SIMULATION OF THE DNP AND ELDOR DATA

Simulations of the field dependence of the ELDOR attenuation and DNP signal enhancement curves in the 4-amino-TEMPO system are performed using the thermodynamic model illustrated in Fig. 12. The inhomogeneous EPR line is split into N bins, each of equal frequency width ω_{bin} .

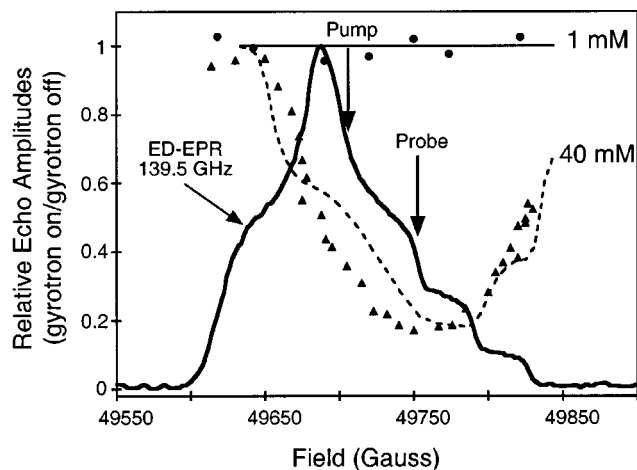


FIG. 11. Experimental data and simulations of the ELDOR echo attenuation as a function of magnetic field for 40 mM (triangles) and 1 mM (circles) 4-amino TEMPO in 60/40 glycerol/water at ~11 K. A ~100 ms 139.64 GHz gyrotron pulse is used for excitation, followed by a 10 μs delay and detection of the stimulated electron spin-echo at 139.5 GHz. The arrows labeled “Pump” and “Probe” are spaced at the frequency difference between the two microwave sources (140 MHz). The 139.5 GHz echo-detected EPR spectrum (the “Probe” frequency) for 1 mM 4-amino TEMPO is shown above the graph. The parameters used to generate the 40 mM simulation (dashed trace) are the same as those used for Fig. 7, except that $W_{mw}=0.1$ MHz to account for the increased microwave power. The 1 mM simulation (solid trace) used the same parameters as the 40 mM simulation, except that the phenomenological bin-to-bin diffusion rate was decreased by a factor of 1600 ($W_{bb}=0.016$ MHz).

Each bin is characterized by an electron Zeeman spin temperature T_i (and $\alpha_i=1/kT_i$) and a center frequency ω_{ei} , and has an intensity (or fraction of total spins) n_i , normalized so $\sum n_i=1$. The fractional number of spins in each bin i (n_i) is obtained from the intensity of the normalized 1 mM 4-amino-TEMPO EPR spectrum. Single parameters β

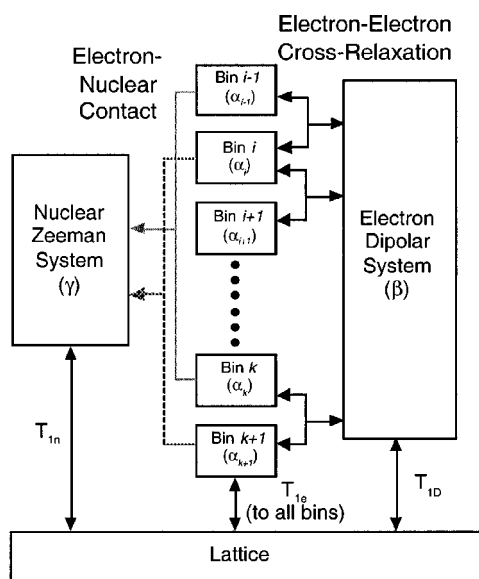


FIG. 12. Thermodynamic model used for the simulations of DNP in the 4-amino TEMPO/water/glycerol system. Each of the N bins represents an equally spaced region of the EPR spectrum. Electron–electron cross-relaxation occurs between neighboring bins and electron–electron–nuclear relaxation occurs between bins spaced ω_n apart.

$=1/kT_{EDS}$ and $\gamma=1/kT_{NZS}$ describe the temperatures of the electron dipolar system and the nuclear Zeeman system, respectively.

Given this model, the dynamics of the spin system can now be described by a set of rate equations characterizing the effects of microwave saturation, electron–electron cross-relaxation, electron–electron–nuclear cross-relaxation, and spin-lattice relaxation. The rates of these processes are derived from the off diagonal terms of the Hamiltonian coupling the various baths as discussed by Provotorov.¹⁴ We define a vector \mathbf{M} , consisting of $N+2$ parameters that completely define the state of the spin system. The first N elements of \mathbf{M} are proportional to the electron Zeeman magnetization in each of the N bins. The final two elements of \mathbf{M} describe the magnetization of the electron dipolar and nuclear Zeeman baths. The rate equations for the time dependence of the different magnetizations are given by

$$\frac{d\mathbf{M}}{dt} = \hat{\mathbf{A}}\mathbf{M} + \mathbf{B}, \tag{1}$$

where the elements of $\hat{\mathbf{A}}$ and \mathbf{B} are derived from the following relations:

$$\begin{aligned} \frac{d(\hbar\omega_{ei}\alpha_i)}{dt} &= -W_i^{mw} - W_{ei}^{sl} - W_{i-1,i}^{cr} + W_{i,i+1}^{cr} - W_{i-a,i}^{tc} \\ &\quad + W_{i,i+a}^{tc}, \\ \frac{d(\hbar\omega_{bin}\beta)}{dt} &= -W_D^{sl} - \frac{\omega_{bin}^2}{\omega_{loc}^2} \sum_{1 \leq i < N} W_{i,i+1}^{cr}, \\ \frac{d(\hbar\omega_n\gamma)}{dt} &= -W_{nuc}^{sl} - \frac{1}{N} \sum_{1 \leq i < N-a} W_{i,i+a}^{tc}, \end{aligned} \tag{2}$$

where

$$W_i^{mw} = W_{mw}(\hbar\omega_{ei}\alpha_i)$$

for irradiation on resonance with bin i

$$W_i^{mw} = 0 \text{ otherwise,}$$

$$W_{ei}^{sl} = \frac{\hbar\omega_{ei}}{T_{1e}}(\alpha_i - \alpha_i^0),$$

$$W_D^{sl} = \frac{\hbar\omega_{bin}}{T_{1D}}(\beta - \beta^0),$$

$$W_{nuc}^{sl} = \frac{\hbar\omega_n}{T_{1n}^x}(\gamma - \gamma^0),$$

$$W_{i,j}^{cr} = W_{bb}[n_i(\hbar\omega_{ej}\alpha_j) - n_j(\hbar\omega_{ei}\alpha_i) + n_i n_j(\hbar\beta\omega_{bin})],$$

and

$$W_{i,j}^{tc} = W_{een}[n_i(\hbar\omega_{ej}\alpha_j) - n_j(\hbar\omega_{ei}\alpha_i) + n_i n_j(\hbar\gamma\omega_n)].$$

In Eq. (2) ω_n is the nuclear Larmor frequency and a is the number of bins separating spin packets ω_n apart. α_i^0 , β^0 , and γ^0 are the thermal equilibrium values of the inverse spin temperatures α_i , β , and γ . W_{bb} is a phenomenological bin-to-bin diffusion rate constant, $W_{i,j}^{cr}$ is the cross-relaxation rate between bins i and j , W_{een} is the three spin electron–electron–nuclear cross-relaxation rate constant, $W_{i,j}^{tc}$ is the

thermal contact or electron–nuclear polarization transfer rate, and W_{mw} is the microwave saturation rate constant. The spin-lattice relaxation for the electron Zeeman, electron dipolar, and nuclear Zeeman baths are described by W_{ei}^{sl} , W_D^{sl} , and $W_{\text{nuc}}^{\text{sl}}$, respectively, where T_{1e} and T_{1D} are the electronic and dipolar spin-lattice relaxation times and T_{1n}^x is the relaxation time of the nuclear spins arising from processes other than electron–electron–nuclear relaxation. Finally, ω_{loc} is the average electron–electron dipolar frequency (the notation is based on that of Hoogstraate *et al.*²³). We now discuss the important parameters in Eqs. (1) and (2) and the inherent assumptions made in deriving these relations.

A. Frequency bin width

A critical parameter affecting the simulations is the number of bins N into which the spectrum is divided. In our simulations, we have typically split the 4-amino-TEMPO spectrum into 400 bins of width $\omega_{\text{bin}}/2\pi=1.8$ MHz. The bin width is chosen to be much larger than the homogeneous spin packet width (~ 0.25 MHz) for two reasons. First, using the small homogeneous spin packet linewidth as the bin width would require a very large number of bins making calculations unwieldy. Second, the exact shapes of the homogeneous spin packets are unknown. In particular, the long frequency tails of the homogeneous spin packets may extend over many spin packets making the cross-relaxation dynamics more complicated than that described by a simple model of cross-relaxation between neighboring spin packets alone. Using a bin width much larger than the homogeneous spin packet width allows us to simplify the calculations and consider exchange between neighboring bins only. Finally, the bin width is also chosen to be small enough such that the intensity of the 4-amino-TEMPO EPR spectrum is relatively constant across a bin.

B. Microwave saturation

Only allowed transitions are assumed to be driven by the microwave field, as the experiments described here are all performed using sources that generate relatively weak microwave fields. This permits us to neglect the effect of microwave-driven electron–nuclear transitions in the simulations. The microwave field is considered to perturb only the bin with which it is on resonance, which should be a good approximation as the microwave field strength in these experiments is small compared to $\omega_{\text{bin}}/\gamma_e$ and the homogeneous spin packet line width is smaller than the bin width.

Unlike the case of a single homogeneous line, in which off-resonance irradiation of the EPR line drives polarization transfer by perturbing the dipolar spin temperature, we neglect the effect of microwave irradiation on the parameter β . This is reasonable for two reasons. First, microwave irradiation within an inhomogeneous line with unresolved spin packets will result in some spin packets being driven above their resonance frequency and some being driven below their resonance frequency, minimizing the net perturbation of β . Also, the magnitude of any contribution to β from off-resonance irradiation of a narrow spin packet in the TEMPO line should be much less than the effect of cross-relaxation if cross-relaxation is reasonably fast.

The microwave saturation rate constant W_{mw} in the simulations can be estimated as $W_{\text{mw}}=\pi\omega_1^2h(\omega_{\text{mw}})$, where ω_{mw} is the microwave frequency, ω_1 is the electronic Rabi frequency, and $h(\omega)$ is the normalized shape of the bin.^{3,10,14} Since the number of bins is sufficiently large, their shape can be considered effectively rectangular, suggesting $h(\omega_{\text{mw}})\sim 1/\omega_{\text{bin}}$. Because the ELDOR and DNP measurements are performed using a spectrometer that differs greatly from a standard high-field pulsed EPR spectrometer, it is difficult to directly measure ω_1 in either experiment. However, reasonable estimates can be derived by extrapolating from the known Rabi frequency ($\omega_1/2\pi\sim 0.8$ MHz) of the 139.5 GHz pulsed EPR spectrometer which uses the 10 mW Gunn diode source for excitation and a cylindrical resonator as the coupling structure. In the ELDOR experiment, the pump field strength was estimated by accounting for the power of the gyrotron source and accounting for the fact that the resonator is tuned to the probe frequency (139.50 GHz) rather than the pump frequency (139.64 GHz). In the DNP experiment, the microwaves are simply launched into the sample from a WR-8 waveguide. The Q is extremely low with this configuration, and the microwave field is extremely anisotropic, resulting in a wide distribution of relative field strengths.

C. Electron and nuclear spin-lattice relaxation

The electronic spin-lattice relaxation rate ($1/T_{1e}$) was assumed to be approximately constant across the 4-amino-TEMPO EPR spectrum. T_{1e} was determined to be approximately 75 ms at 12 K from experiments on low-concentration (1 mM) samples and long-saturation pulse saturation-recovery measurements on the 40 mM 4-amino-TEMPO solution. The electron dipolar relaxation time (T_{1D}) is difficult to measure directly, but is typically taken to be a factor of 1–3 times shorter than T_{1e} .²⁴ The observed nuclear spin-lattice relaxation rate ($1/T_{1n}$) can be shown to be equal to

$$\frac{1}{T_{1n}} = \frac{1}{T_{1n}^x} + \frac{1}{T_{nee}} \quad (3)$$

assuming that relaxation of the electronic system is not the bottleneck in the nuclear relaxation process. In Eq. (3), T_{nee} is the rate constant for the polarization transfer from the EDS to the NZS due to electron–electron–nuclear relaxation, and T_{1n}^x is the spin-lattice relaxation time for the NZS arising from processes other than the electron–electron–nuclear flip–flops. Measurements of the nuclear relaxation rate at low electron concentrations can help to determine the value of T_{1n}^x at high concentrations, although it is important to recognize that direct electron–nuclear relaxation processes also contribute to T_{1n}^x .

In the solution of the equation of motion for the spin system [Eq. (1)], the assumption is often made that the electronic system reaches a steady-state much faster than the nuclear system, allowing the electronic steady-state solution to be used to determine the nuclear dynamics. We have also made this assumption for the simulations of the 4-amino

TABLE I. Parameters used to simulate the ELDOR and DNP data along with their method of determination.

Parameter	Value	Method of determination
n_i		Normalized 1 mM TEMPO CW-EPR spectrum
δ	720 MHz	Full CW-EPR linewidth
N	400	...
$\omega_{\text{bin}}/2\pi$	1.8 MHz	δ/N
$\omega_n/2\pi$	211 MHz	Determined by external magnetic field
$\omega_{\text{loc}}/2\pi$	20 MHz	Estimate from TEMPO concentration
T_{1D}	25 ms	Estimate ($T_{1e}/3$)
T_{1e}	75 ms	Saturation-recovery EPR
W_{mw} (ELDOR)	0.1 MHz	Estimate from known
(DNP)	0.0005 MHz	power and resonator Q
W_{bb} (40 mM)	25 MHz	Best fit of ELDOR and
(1 mM)	0.016 MHz	DNP field dependencies

TEMPO system. In general, the conditions for the validity of this assumption are difficult to derive, but for the special case of fast cross-relaxation, they are

$$(T_{1e})^{-1} \gg C_n (T_{1n})^{-1}, \quad (4)$$

and

$$(T_{1D})^{-1} \gg \frac{C_n \omega_n^2}{\omega_{\text{loc}}^2} (T_{nee} + T_{1n}^x)^{-1},$$

where ω_{loc} represents the magnitude of the non-Zeeman Hamiltonian and C_n is the ratio of the number of nuclear spins to the number of electron spins.¹² For the 40 mM 4-amino-TEMPO/water/glycerol system, we have estimated that this condition is not held sufficiently strongly to guarantee that the electronic dynamics are unaffected by electron–nuclear processes (see Table I). However, we have observed no significant differences in the calculated electronic steady-state polarizations in the ELDOR and DNP simulations when the coupling to the nuclear spins is incorporated into the simulations. Therefore, we have employed the electronic steady-state approximation, which reduces the number of free parameters in the simulations.

D. Electron–electron cross-relaxation

As initially described by Bloembergen *et al.*,¹⁷ spin packets that overlap in frequency space can exchange polarization via energy conserving flip–flop processes. The rate of cross-relaxation ($1/\tau_{\text{cr}}$) between two spin-1/2 electrons (S_i and S_j) depends on the magnitude of the flip–flop term [$B_{ij}(S_i^+ S_j^- + S_i^- S_j^+)$] of the dipolar Hamiltonian and the spectral overlap between the two packets. For a crystalline system consisting of two coupled electrons, each displaying a homogeneous EPR line with center frequencies ω_{S_i} and ω_{S_j} , respectively, this rate can be approximated as

$$\frac{1}{\tau_{\text{cr}}} = 2\pi |B_{ij}|^2 g_{ij}(\Delta), \quad (5)$$

where

$$B_{ij} = -\frac{1}{4} \frac{\gamma_e^2 \hbar}{r^3} (1 - 3 \cos^2 \theta), \quad (6)$$

$$g_{ij}(\Delta) = \int_{-\infty}^{\infty} g_i(\omega) g_j(\omega') \delta(\omega - \omega' - \Delta) d\omega d\omega', \quad (7)$$

r and θ are coordinates of the vector between the two electrons with respect to the external magnetic field, and $g_i(\omega)$ and $g_j(\omega')$ are the normalized [$\int_{-\infty}^{\infty} g(\omega) d\omega = 1$] spin packet line shapes.^{17,25,26} The flip–flop transition removes Zeeman energy $\hbar\omega_{S_i}$ from one spin packet and delivers $\hbar\omega_{S_j}$ to the other spin packet. The difference in energy [$\hbar\Delta = \hbar(\omega_{S_i} - \omega_{S_j})$] which emerges from the cross-relaxation process is taken up by the electron–electron dipolar reservoir. Thus, cross-relaxation transitions perturb the Zeeman temperatures of the two spin packets and the temperature of the dipolar broadening system.

As mentioned earlier, in our simulations we have made the simplifying approximation of using a bin width that is greater than the homogeneous spin packet linewidth. This allows us to consider only cross-relaxation between neighboring frequency bins. Since the homogeneous electronic spin packet linewidth is much smaller than the width of a bin, this is likely to be a reasonable assumption. However, if the spin packets have a long, high frequency tail, which is difficult to measure in our spectrometer due to receiver ring-down, long-range processes may play a significant role.

Since ω_{bin} is much greater than the spin packet linewidth, the parameter W_{bb} in the simulation does not represent the rate of exchange between two homogeneous spin packets separated by ω_{bin} ; rather, it is simply a phenomenological spin diffusion rate constant between the spin packets in one bin with those in the neighboring bin. We make the assumption that W_{bb} is constant across the spectrum, which is reasonable since the spin packet line shapes are approximately the same across the entire EPR line, implying that the overlap integrals [see Eq. (7)] between spin packets are also uniform across the EPR line.

It should be noted that the fact that W_{bb} is constant across the line does not imply that the observed rate of polarization diffusion will be uniform. The actual cross-relaxation rate, $W_{i,j}^{\text{cr}}$, depends not only on W_{bb} , but also on the number of spins n_i and n_j , which differ across the EPR line [see Eq. (2)], and on the magnetization m_i and m_j (where $m_i = \hbar\omega_i\alpha_i$). In the center of the EPR line, where the intensity is largest, the likelihood of an electron spin being spatially proximate to another electron spin close in frequency is much larger than on the edge of the line. This results in more rapid cross-relaxation in the center of the line than on the edge. Because this rate is difficult to predict *a priori*, W_{bb} is determined by fitting the simulations to the experimental ELDOR and DNP enhancement field dependence data.²³

E. Electron–electron–nuclear relaxation

The electron–nuclear thermal contact is mediated by the electron–electron–nuclear relaxation [W_{een} , see Eq. (2)]. In

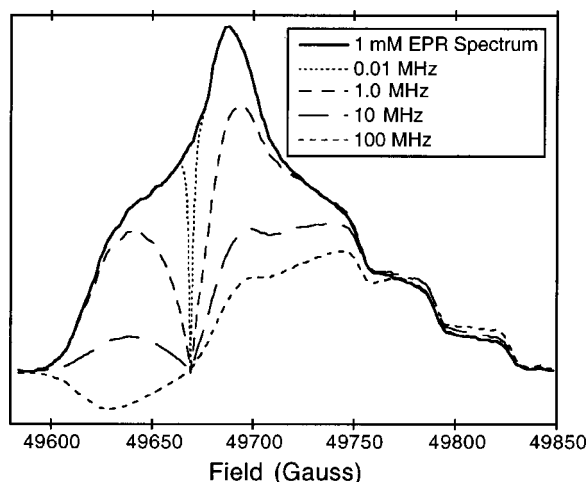


FIG. 13. Simulations of hole-burning in the 4-amino TEMPO EPR line as a function of the phenomenological bin-to-bin diffusion rate W_{bb} . The EPR spectrum is calculated under conditions of steady-state microwave irradiation using estimated parameters for a 40 mM solution of the radical at 12 K (see Table I). The parameters used in the simulations are $\omega_{mw}=49670$ G, $T_{1e}=75$ ms, $T_{1D}=25$ ms, $\omega_{loc}/2\pi=20$ MHz, and $W_{mw}=0.1$ MHz. The solid line shows the echo-detected EPR spectrum of 1 mM 4-amino TEMPO in 60:40 glycerol/water.

our simulations we assume that only those spin packets that differ in frequency by exactly ω_n contribute to this three-spin relaxation process.

V. DISCUSSION

Thermal mixing relies on a strong microwave induced perturbation of the EDS and good thermal contact between the EDS and the NZS. These conditions are satisfied for a homogeneous EPR line where the nuclear Zeeman frequency is less than the homogeneous EPR linewidth. In contrast, the EPR spectrum of 1 mM 4-amino-TEMPO shown in Fig. 7 (top) clearly displays evidence of inhomogeneous broadening from both electron g -anisotropy and, in the high field region, ^{14}N hyperfine coupling. As discussed earlier, electron–electron cross-relaxation could render the EPR line effectively homogeneous on the DNP time scale providing a mechanism for thermal mixing.

Figure 13 shows a series of simulations of EPR hole-burning under a reasonably strong microwave field. Estimated values of T_{1e} , T_{1D} and ω_{loc} for the 4-amino-TEMPO system at 12 K are used, and the phenomenological bin-to-bin spin diffusion rate (W_{bb}) is varied over several orders of magnitude. 139.50 GHz microwave irradiation at a magnetic field of 49 670 Gauss is employed in the simulations. For slow cross-relaxation rates, there is little spectral diffusion, and the line can be considered strictly inhomogeneous. As the cross-relaxation rate increases, the line becomes increasingly homogeneous, until, under very rapid cross-relaxation, the hole is completely delocalized, and the downfield portion of the EPR line becomes emissive. In this limit, the polarization ($p_i=m_i/n_i$) is linear across the entire line, meaning that the dipolar broadening reservoir can be described by a single parameter β . The mechanism for this effect in the simulation is the cooling of the electronic dipolar reservoir by asymmetric cross-relaxation (due to the off-center irradiation of the

EPR line). Since this reservoir couples all neighboring pairs of spin packets, the cooling of the dipolar reservoir drives all pairs toward an equal polarization difference.

Experimental evidence of electron–electron cross-relaxation is, however, difficult to obtain. Unlike NMR experiments, where the entire spin system can be excited with a single pulse (and spectral diffusion processes across the entire line can be directly monitored), the excitation bandwidth of high-frequency EPR sources is frequently orders of magnitude narrower than the spectral width of the EPR line. Because the microwave sources are of fixed frequency, and the magnetic field sweep rate is not sufficiently fast to monitor spectral diffusion across the entire EPR line, there are limited options to measuring the cross-relaxation dynamics. However, electron–electron double resonance (ELDOR) and saturation-recovery EPR experiments can provide this kind of information.

A. Electron–electron double resonance (ELDOR)

ELDOR experiments monitor the rate of cross-relaxation between two fixed-frequency microwave sources; in this case the 139.5 GHz Gunn diode and the 139.64 GHz gyrotron. Since this frequency difference (140 MHz) corresponds to approximately one fourth of the width of the entire EPR line, this implementation should be a useful monitor of medium-range spectral diffusion across the 4-amino-TEMPO EPR line. Clear evidence of electron cross relaxation is observed in Fig. 11 for 40 mM TEMPO. However, the strong field dependence of the echo attenuation at the probe position due to the pump pulse indicates that cross-relaxation is fastest in the center of the line, where the greatest density of spin packets resides. This anisotropy in the ELDOR data clearly indicates that the cross-relaxation rate is in the intermediate regime and is not significantly faster than $1/T_{1e}$ or $1/T_{1D}$.

Using the simulation methods presented in Sec. IV, we were able to obtain reasonable fits for the ELDOR data (Fig. 11). The ELDOR simulation is produced by calculating the electronic spin polarization at 139.5 GHz under a CW microwave pulse at 139.64 GHz. The CW approximation is appropriate since the length of the pump pulse (100 ms) is longer than the EPR spin-lattice relaxation time (75 ms) and since increasing the microwave pulse length did not affect the experimental results. A phenomenological bin-to-bin diffusion rate (W_{bb}) of 25 MHz was used for the simulation of the 40 mM 4-amino-TEMPO ELDOR data. The parameters used in the simulation are tabulated in Table I. The small discrepancy between the 40 mM 4-amino-TEMPO experimental and simulated ELDOR curves observed in the center of the EPR line may arise from a number of factors. In the simulations we have assumed a homogeneous electron spin-lattice relaxation time T_{1e} , while saturation-recovery EPR measurements of T_{1e} indicate that there is a slight anisotropy in T_{1e} . To fit the edges of the ELDOR curve, where T_{1e} is somewhat longer than used in the simulations, would require a slower cross-relaxation rate than that used for the center of the line. Furthermore, the gyrotron frequency is not locked and a small drift in the gyrotron frequency, due to cavity heating (see Sec. II), for example, could also lead to a distortion of the ELDOR curve. Finally, the simple model for

the cross-relaxation, in which only nearest neighbor spin packet interactions are considered, may not work as well for the edges of EPR line, where the long frequency tail of electron spin packets would become more important for cross-relaxation than in the center of the line.

To check our estimate of the 40 mM 4-amino-TEMPO cross-relaxation rate, we calculated the 1 mM ELDOR curve by decreasing the phenomenological bin-to-bin rate W_{bb} used in the 40 mM simulation by a factor of 1600. This is justified by the fact that the cross-relaxation rate is proportional to the square of the average dipolar coupling between electronic spins [see Eq. (5)], which is in turn proportional to the concentration of electrons. The simulations predict that no ELDOR echo attenuation should be observed in the 1 mM solution, consistent with experimental observations.

The phenomenological bin-to-bin spin diffusion rate constant W_{bb} is related to the electron-electron dipolar coupling (ω_{ee}), which drives the electron cross-relaxation. Abragam gives an estimate for the electron-electron dipolar broadening in a magnetically dilute substance in which the magnetic moments are distributed randomly,

$$\omega_{ee} = \frac{1}{T_{2e}^{ee}} \cong 3.8 \gamma_e^2 \hbar N_e, \quad (8)$$

where N_e is the density of the electron spins.²⁷ The rate ω_{ee} should be on the order of an upper bound for W_{bb} , as this is the maximum rate at which electrons that are on-resonance with one another will undergo flip-flop transitions. For a 40 mM solution, this results in a maximal rate constant W_{bb} of about 35 MHz consistent with our value of 25 MHz determined from the simulation of the ELDOR data. For the inhomogeneously broadened 4-amino-TEMPO EPR line only a small fraction of the spins are on resonance which is accounted for in the cross-relaxation rate $W_{i,j}^{cr}$ of Eq. (2) by weighing W_{bb} by the number of spins n_i on resonance. The electron-electron dipolar coupling also contributes to the electron spin-echo phase memory time (T_m); however only those spins that are on resonance will drive the phase-memory relaxation. The electron phase-memory relaxation rate constant ($1/T_m = 250$ kHz) therefore provides an upper bound for the weighted electron-electron dipolar relaxation rate constant, $n_i W_{bb}$. For the center of the EPR line a rate constant of $n_i W_{bb} \sim 168$ kHz is obtained, consistent with the phase-memory rate upper bound.

B. Saturation-recovery EPR

The pulsed saturation-recovery EPR experiments also suggest that electron cross-relaxation plays an important role in the spin dynamics. Saturation-recovery EPR measurements monitor the rate at which a hole returns to thermal equilibrium after a saturation pulse, using a single microwave source for excitation and detection. Both electron spin-lattice relaxation and electron cross-relaxation can contribute to the relaxation. The saturation-recovery curves for the 40 mM solution (Figs. 9 and 10) show large variations both as a function of saturating pulse length and the magnetic field position, while such effects in the 1 mM curves (Fig. 8) are much less pronounced. After the saturating microwave pulse,

two processes can lead to recovery of the spin polarization: cross-relaxation with other spin packets in the EPR line and spin-lattice relaxation. Cross-relaxation processes will only affect the recovery curves if there is communication between the observed spin packet and other spin packets at a rate faster than spin-lattice relaxation, and if these other spin packets are at a different spin temperature from the observed spin packet. This condition will be met when the saturation pulse is not sufficiently long for cross-relaxation to proceed fully to all coupled spins.

The 1 mM solution displays pure single-exponential recovery for a range of saturating pulse lengths and line positions. The relaxation is slightly faster with the 10 ms pulse than with the 60 ms pulse. This could arise from a small component of the relaxation being attributed to electron cross-relaxation. It is also possible that instantaneous²⁸ diffusion contributes to the faster relaxation for the 10 ms saturation pulse data. The fact that the effect of cross-relaxation may be visible in the 1 mM saturation recovery data and not in the corresponding ELDOR data is not surprising, given that ELDOR probes diffusion over a large frequency range, while the saturation-recovery experiment probes the cross-relaxation to spins near in frequency.

In contrast, the relaxation dynamics of the 40 mM solution show a strong dependence both on the magnetic field strength and the saturating pulse length. For short saturating pulses, we observe two relaxation components: a fast component that can be attributed to cross-relaxation, and a slower component that can be attributed to pure T_{1e} relaxation. As the saturating pulse length increases, the longer relaxation component begins to dominate, until, when the saturating pulse length is on the order of the spin-lattice relaxation time, the recovery curves become single-exponential. The long pulse saturates not only the spin packet on resonance, but also the entire cross-relaxation channel, so that pure T_{1e} relaxation is observed. This effect is exhibited for irradiation at two line positions, 49 634 G (Fig. 9), which corresponds to the low-field edge of the EPR line, and 49 690 G (Fig. 10), which is approximately the first moment of the EPR spectrum.

An interesting difference between the data for the two magnetic field values is that the saturation-recovery curves for the 49 634 G position vary substantially as a function of saturating pulse length until the pulse is on the order the spin-lattice relaxation time (~ 75 ms). However, under irradiation at the center of the EPR line, the recovery curves become invariant for much shorter saturating pulse lengths (≥ 10 ms). This suggests that, in the center of the line, the cross-relaxation time to most of the spin packets in the line is below 10 ms, while at the low-field edge, there is a large range of cross-relaxation times, up to the spin-lattice relaxation time. This effect is even more pronounced on the high field edge (data not shown). These observations are again consistent with fast cross-relaxation in the center of the line, while the edges the EPR line, where the spectral density is much lower, remain partially inhomogeneous.

C. Dynamic nuclear polarization

Both the ELDOR and the saturation-recovery EPR measurements suggest that a simple picture of a purely homogeneous or inhomogeneous EPR line will not suffice to model the DNP effect in 4-amino-TEMPO. Thus, our attempts to simulate the DNP and ELDOR experiments using a model in which cross-relaxation is in the fast limit were unsuccessful.

The field dependence of the DNP enhancement is calculated in two steps, using the formalism developed in the Sec. IV and the parameters determined from the ELDOR and saturation-recovery EPR data (see Table I). First the steady-state solution for the electronic system under microwave irradiation is determined without considering couplings to the nuclear spins. This steady-state solution is then used in the rate equation describing the time-dependence of the nuclear magnetization in Eq. (2). If we assume the initial nuclear polarization is small, then the steady-state nuclear polarization, or DNP enhancement ϵ , will simply be proportional to the total electron polarization ($p_i^{ss} = m_i^{ss}/n_i$) differences among all spin pairs ω_n apart,

$$\epsilon \propto \frac{T_{1n}^x W_{een}}{N} \sum_{1 \leq i \leq N-a} n_i n_{i+a} (p_i^{ss} - p_{i+a}^{ss}). \quad (9)$$

Because of the difficulty in measuring T_{1n}^x and W_{een} , we determine the shape of the enhancement curve as a function of magnetic field strength from the sum of the weighted ($n_i n_{i+a}$) polarization differences and normalize this curve to the experimental data. Using the simulation parameters of Table I and a saturation parameter of $W_{mw} = 0.0005$ MHz, we obtain an excellent fit of the field dependence of the DNP enhancement as demonstrated in Fig. 10. The DNP field dependence simulations are extremely dependent on the microwave saturation parameter W_{mw} . In Fig. 11, structure is clearly evident on the high field edge of the DNP field dependence and the maximal signal enhancement is about 15. In experiments employing the high power gyrotron and in simulations using larger saturation parameters some of the structure in the DNP field dependence is no longer evident (data not shown). The larger DNP enhancements obtained experimentally with the gyrotron^{5,6,8} also indicate an increased saturation of the EPR line. The saturation parameter used to simulate the DNP enhancement curve is much smaller than that used for the ELDOR curve. This observation is consistent with the decreased microwave power available from the Gunn Diode (~ 10 mW) and the lack of a microwave resonant structure for the DNP/NMR probe (see Experiment).

The simulation of the DNP field dependence curve utilizes the same set of parameters (see Table I) as the ELDOR field dependence simulation for the cross-relaxation rate, electron spin-lattice relaxation rate, and relative heat capacities of the various baths. Only the microwave saturation parameters change between the different experiments. The phenomenological bin-to-bin diffusion rate constant of $W_{bb} = 25$ MHz was determined from the best fit of both the DNP and ELDOR curves, and the rest of the parameters were estimated as discussed earlier. The simultaneous fitting of the two data sets provides added confidence in the uniqueness of

the fits and the determination of the simulation parameters. The fact that excellent fits are obtained for both data sets suggest that our simplified model of the electron cross-relaxation adequately describes the spin dynamics of the 4-amino-TEMPO system.

VI. CONCLUSIONS

We have presented a model for analyzing polarization transfer via thermal mixing at high magnetic field strengths which accounts for electron-electron cross-relaxation within an inhomogeneously broadened EPR line and have applied this model to simulate DNP and ELDOR experiments in the 4-amino-TEMPO system. These studies indicate that for 40 mM 4-amino-TEMPO, the EPR line is in the intermediate cross-relaxation regime, and thus the three-bath thermal mixing model, used previously to describe low field experiments, does not adequately explain the polarization dynamics of the system at high fields. Instead, electron cross-relaxation must be explicitly included to model the coupling between the electronic and nuclear spins. In this case the polarization transfer proceeds via spin flip-flops between pairs of electronic spin packets, spaced ω_n apart, whose Zeeman temperatures can differ from one another. Both the field dependence of the DNP enhancement and the ELDOR data are accurately simulated using this model of electron cross-relaxation and help to explain the dramatic enhancements that have been observed previously at high magnetic fields with the inhomogeneously broadened 4-amino TEMPO free radical.

ACKNOWLEDGMENTS

We gratefully acknowledge the support of the National Institutes of Health by Grants Nos. GM-38352 and RR-00995. C.T.F. was supported by a NIH Postdoctoral Fellowship (GM-18790). We thank Marina Bennati, Melanie Rosay, and Volker Weis for numerous helpful discussions.

- ¹A. E. Bennett, R. G. Griffin, and S. Vega, *NMR Basic Princ.* **33**, 1 (1994).
- ²K. Schmidt-Rohr, *Macromolecules* **29**, 3975 (1996).
- ³A. Abragam and M. Goldman, *Nuclear Magnetism: Order and Disorder* (Clarendon, Oxford, 1982).
- ⁴C. P. Slichter, *Principles of Magnetic Resonance*, 3rd ed. (Springer-Verlag, Berlin, 1990).
- ⁵L. R. Becerra, G. J. Gerfen, B. F. Bellew *et al.*, *J. Magn. Reson., Ser. A* **117**, 8 (1995).
- ⁶G. J. Gerfen, L. R. Becerra, D. A. Hall, D. J. Singel, and R. G. Griffin, *J. Chem. Phys.* **102**, 9494 (1995).
- ⁷V. Weis, M. Bennati, M. Rosay, J. A. Bryant, and R. G. Griffin, *J. Magn. Reson.* **140**, 293 (1999).
- ⁸L. R. Becerra, G. J. Gerfen, R. J. Temkin, D. J. Singel, and R. G. Griffin, *Phys. Rev. Lett.* **71**, 3561 (1993).
- ⁹K. E. Kreisler, C. T. Farrar, R. G. Griffin, and R. J. Temkin, in *Proceedings of the 23rd International Conference on Infrared and Millimeter Waves*, 1998, p. 357.
- ¹⁰M. Goldman, *Spin Temperature and Nuclear Magnetic Resonance in Solids* (Oxford University Press, London, 1970).
- ¹¹W. T. Wenckebach, T. J. B. Swanenburg, and N. J. Poulis, *Phys. Rep.* **14**, 181 (1974).
- ¹²M. J. Duijvestijn, R. A. Wind, and J. Smidt, *Physica B* **138**, 147 (1986).
- ¹³R. A. Wind, M. J. Duijvestijn, C. van der Lugt, A. Manenschijn, and J. Vriend, *Prog. Nucl. Magn. Reson. Spectrosc.* **17**, 33 (1985).
- ¹⁴B. N. Provotorov, *Sov. Phys. JETP* **14**, 1126 (1962).
- ¹⁵L. L. Buishvili, *Sov. Phys. JETP* **22**, 1277 (1966).

- ¹⁶W. T. Wenckebach, G. M. van den Heuval, H. Hoogstraate, T. J. B. Swanenburg, and N. J. Poulis, *Phys. Rev. Lett.* **22**, 581 (1969).
- ¹⁷N. Bloembergen, S. Shapiro, P. S. Pershan, and J. O. Artman, *Phys. Rev.* **114**, 445 (1959).
- ¹⁸V. A. Atsarkin, A. E. Mefed, and M. I. Rodak, *Phys. Lett.* **27A**, 57 (1968).
- ¹⁹V. A. Atsarkin, *Sov. Phys. JETP* **31**, 1012 (1970).
- ²⁰M. I. Rodak, *Sov. Phys. Solid State* **15**, 290 (1973).
- ²¹V. A. Atsarkin, *Sov. Phys. Usp.* **21**, 725 (1978).
- ²²S. Un, J. Bryant, and R. G. Griffin, *J. Magn. Reson., Ser. A* **101**, 92 (1993).
- ²³H. Hoogstraate, J. van Houten, L. A. H. Schreurs, W. T. Wenckebach, and N. J. Poulis, *Physica (Utrecht)* **65**, 347 (1973).
- ²⁴V. A. Atsarkin and M. I. Rodak, *Sov. Phys. Usp.* **15**, 251 (1972).
- ²⁵P. S. Pershan, *Phys. Rev.* **117**, 584 (1960).
- ²⁶M. Hirono, *J. Phys. Soc. Jpn.* **16**, 766 (1961).
- ²⁷A. Abragam, *The Principles of Nuclear Magnetism* (Clarendon, Oxford, England, 1961).
- ²⁸M. K. Bowman and L. Kevan, in *Time Domain Electron Spin Resonance*, edited by L. Kevan and R. N. Schwartz (Wiley, New York, 1979), pp. 67–105.